Cell Reports Medicine, Volume *3*

Supplemental information

Spatial heterogeneity of infiltrating T cells in high-grade serous ovarian cancer revealed by multi-omics analysis

Bin Yang, Xiong Li, Wei Zhang, Junpeng Fan, Yong Zhou, Wenting Li, Jingjing Yin, Xiaohang Yang, Ensong Guo, Xi Li, Yu Fu, Si Liu, Dianxing Hu, Xu Qin, Yingyu Dou, Rourou Xiao, Funian Lu, Zizhuo Wang, Tianyu Qin, Wei Wang, Qinghua Zhang, Shuaicheng Li, Ding Ma, Gordon B. Mills, Gang Chen, and Chaoyang Sun

Spatial Heterogeneity of Infiltrating T cells in High-Grade Serous Ovarian Cancer revealed by Multi-omics analysis

Authors and Affiliations

Bin Yang[1#], Xiong Li[2#], Wei Zhang[3#], Junpeng Fan[1#], Yong Zhou[3], Wenting Li[1], Jingjing Yin[1], Xiaohang Yang[1], Ensong Guo[1], Xi Li[1], Yu Fu[1], Si Liu[1], Dianxing Hu[1], Xu Qin[1], Yingyu Dou[1], Rourou Xiao[1], Funian Lu[1], Zizhuo Wang[1], Tianyu Qin[1], Qinghua Zhang[2], Shuaicheng Li[3], Ding Ma[1], Gordon B. Mills[4,5], Gang Chen[1*], Chaoyang Sun[1*]

1. Department of Obstetrics and Gynecology, Tongji Hospital, Tongji Medical College, Huazhong University of Science and Technology, Wuhan 430030, China.
2. Department of Gynecology & Obstetrics, the Central Hospital of Wuhan, Tongji Medical College, Huazhong University of Science and Technology, Wuhan, P.R. China.
3. City University of Hong Kong, Shenzhen Research Institute, Shenzhen 518083, China.
4. Department of Cell, Development and Cancer Biology, Oregon Health and Sciences University, Portland, OR 97201, USA; Knight Cancer Institute, Portland, OR 97201,
5. Department of Systems Biology, University of Texas MD Anderson Cancer Center, Houston, TX 77030, USA.

# These authors contribute equally

Supplementary Table 1. Treatment-naive HGSOC sampling and bio-informative data. Related to Figure 1 and Figure 2.

CASE_ID	AGE	DIAGNOSIS	STAGE	SITE	scRNA-seq CELL NUMBER	WGS	RNA-seq	TCR-seq	IHC	Tumor Purity	HRD score	TMB
OV001	53	HGSOC	IIIC	OV001-M_O	-	No	No	YES	YES	0	-	-
				OV001-T_L	-	YES	YES	YES	YES	0.2	11	0.8257
				OV001-M_P1	-	YES	YES	YES	YES	0.4	16	0.8646
				OV001-M_P2	-	YES	YES	YES	YES	0.8	15	0.8668
				OV001-M_A	-	YES	YES	YES	YES	0.2	7	0.8525
				OV001-B	-	YES	No	No	No	-	-	-
OV002	58	HGSOC	IIIC	OV002-T_L	-	YES	YES	YES	YES	0.9	55	1.5346
				OV002-T_R	-	YES	YES	YES	YES	0.9	52	1.5439
				OV002-M_O1	-	YES	YES	YES	YES	0.9	53	1.6254
				OV002-M_O2	-	YES	YES	YES	YES	0.2	23	1.4000
				OV002-M_O3	-	YES	YES	YES	YES	0.4	47	1.4561
				OV002-M_P	-	YES	YES	YES	YES	0.9	54	1.6157
				OV002-B	-	YES	No	No	No	-	-	-
OV003	65	HGSOC	IIIA	OV003-M_A	-	YES	YES	YES	YES	0.8	57	2.0129
				OV003-T_R1	-	YES	YES	YES	YES	0.8	65	2.0486
				OV003_T_R2	-	YES	YES	YES	YES	0.8	62	1.9839
				OV003-B	-	YES	No	No	No	-	-	-
OV004	25	HGSOC	IIIB	OV004-T_L1	10017	YES	YES	YES	YES	0.9	53	1.5425
				OV004-M_P	6761	YES	YES	YES	YES	0.5	45	1.7114
				OV004-T_L2	5285	YES	YES	YES	YES	0.9	52	1.4589
				OV004-T_R	3428	YES	YES	YES	YES	0.9	52	1.4857
				OV004-B	-	YES	No	No	No	-	-	-

OV005	41	HGSOC	IIC	OV005-T_L	5777	YES	YES	YES	YES	0.9	74	3.3729
				OV005-T_R2	5961	YES	YES	YES	YES	0.9	72	3.4000
				OV005-T_R1	5417	YES	YES	YES	YES	0.9	75	3.3139
				OV005-M_P	6331	YES	YES	YES	YES	0.6	76	3.1675
				OV005-B	11681	YES	No	No	No	-	-	-
OV006	52	HGSOC	IIA	OV006-T_L	10864	YES	YES	YES	YES	0.7	22	0.7068
				OV006-T_R	7776	YES	YES	YES	YES	0.9	13	0.8018
				OV006-B	12398	YES	No	No	No	-	-	-
OV008	70	HGSOC	IIIC	OV008-B	10430	YES	No	No	No	-	-	-
				OV008-T_L	-	YES	YES	YES	YES	0.3	-	2.4261
				OV008-T_R	4513	YES	YES	YES	YES	0.4	58	2.4514
				OV008-M_O1	9480	YES	YES	YES	YES	0.2	49	2.2689
				OV008-M_O2	6454	YES	YES	YES	YES	0.2	50	2.3221
				OV008-M_O3	7973	YES	YES	YES	YES	0.2	57	2.3050
OV009	49	HGSOC	IIIC	OV009-B	4917	YES	No	No	No	-	-	-
				OV009-T_L	9113	No	No	YES	YES	0	-	-
				OV009-T_R	8917	YES	YES	YES	YES	0.6	72	2.8246
				OV009-M_O1	6512	YES	YES	YES	YES	0.1	55	2.5175
				OV009-M_O2	5621	YES	YES	YES	YES	0.4	73	3.3479
				OV009-M_P	4881	No	No	YES	YES	0	-	-
OV010	66	HGSOC	IIIC	OV010-M_O1	7592	YES	YES	YES	YES	0.4	71	4.2043
				OV010-T_R2	8312	No	No	YES	YES	0	-	-
				OV010-M_O2	9915	YES	YES	YES	YES	0.2	61	3.9368
				OV010-T_R1	10924	YES	YES	YES	YES	0.4	71	4.1718
				OV010-M_A	10591	YES	YES	YES	YES	0.15	68	3.9132
				OV010-B	9928	YES	No	No	No	-	-	-

M/T:Metastatic/situ lesion，_TR/L:Right ovary/Left ovary，_O/P/A: Omentum/pelvic/abdominic metastatic. POD:progressive disease or death due to progressive disease

Supplementary Table 2. Single cell RNA-seq quality control processing. Related to Figure 2.

Sample	Raw cells	Mean UMIs	Mean genes	Cells (MT>20%)	Doublets	N.O. of non-Tcells[a]	N.O. of T cells
OV004-M-P	8567	4542	1593	157	420	71	6761
OV004-T-L1	12269	4805	1661	184	603	54	10017
OV004-T-L2	8851	4154	1513	271	427	104	5285
OV004-T-R	5146	3975	1426	113	250	47	3428
OV005-B	12805	4758	1419	322	624	1	11681
OV005-M-P	8646	4477	1423	642	400	1	6331
OV005-T-L	8285	5369	1665	739	375	16	5777
OV005-T-R1	7902	6417	1870	1004	340	18	5417
OV005-T-R2	8670	6057	1799	1080	376	27	5961
OV006-B	13342	4579	1506	92	662	6	12398
OV006-T-L	13944	5045	1637	284	681	62	10864
OV006-T-R	10544	4818	1577	495	470	8	7776
OV008-B	11168	4911	1605	34	557	1	10430
OV008-M-O1	11622	5307	1638	467	556	18	9480
OV008-M-O2	8265	4179	1486	413	392	1	6454
OV008-M-O3	10493	3564	1332	454	502	5	7973
OV008-T-R	5272	7137	2110	80	259	6	4513
OV009-B	5905	4695	1360	226	284	1	4917
OV009-M-O1	8667	5725	1631	520	406	2	6512
OV009-M-O2	7982	4807	1497	292	384	35	5621
OV009-M-P	6424	4523	1533	192	311	1	4881
OV009-T-L	12190	4753	1654	1334	541	2	9113
OV009-T-R	11623	4869	1731	809	540	0	8917
OV010-B	10715	5336	1745	22	534	3	9928
OV010-M-A	13157	4738	1622	182	648	0	10591
OV010-M-O1	9568	5072	1771	216	467	4	7592

OV010-M-O2	11941	5320	1814	206	586	6	9915
OV010-T-R1	13413	5954	1809	258	656	11	10924
OV010-T-R2	10180	6024	1832	285	494	2	8312

[a]: the definition of non-T cells is description in Method section "scRNA/TCR-seq data processing"; UMI: Unique Molecular Identifier; MT: mitochondria

Supplementary Table 3. Treatment-naive HGSOC sampling for flow cytometry analysis. Related to Figure 2.

CASE_ID	AGE_AT_DIAGNOSIS	DIAGNOSIS	STAGE	SITE
P1	56	HGSOC	IVB	P1-T_R
				P1-T_L
				P1-M_O
P2	55	HGSOC	IIIC	P2-M_O
				P2-T_R
				P2-T_L
P3	52	HGSOC	IIIC	P3-T_L
				P3-M_O
P4	49	HGSOC	IIIC	P4-M_O
				P4-T_L
P5	51	HGSOC	IIIC	P5-M_O
				P5-T_R
				P5-T_L

M/T:Metastatic/situ lesion, _TR/L:Right ovary/Left ovary, _O: Omentum metastatic.

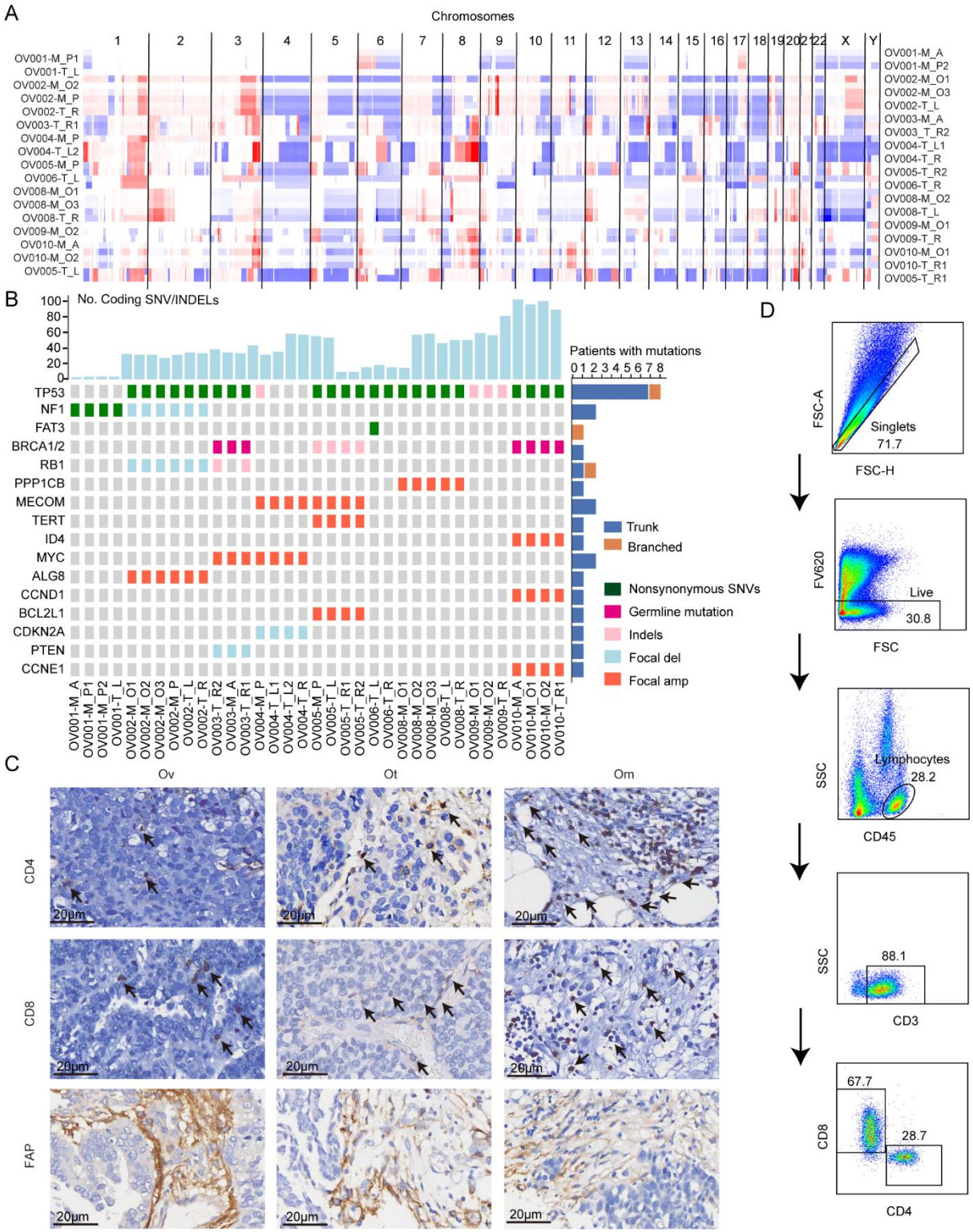

Figure S1. Sample CNV and mutations overview. Related to Figure 1.

A. DNA copy number profiles of all tumor samples of the HGSOC. M/T: Metastatic/ovarian lesion, _TR/L: Right ovary/Left ovary, _O/P/A: Omentum/pelvic/abdominic metastatic. **B.** The distribution of driver mutations across multi-region from 9 OV patients. The upper panel displays the number of coding mutations in each region; the bottom panel shows the mutation types of driver genes and the prevalence of driver genes

shown on the left. M_A = abdominal metastasis; M_P = pelvic metastasis; M_O = omental lesions; T_L = left ovarian lesions; T_R = right ovarian lesions. **C.** Representative images of IHC with indicated antibodies in tumor tissues (200x). Arrows indicate typical T cells. ovarian (Ov), omental (Om), and other distant metastatic (Ot). **D.** CD4 and CD8 T cells, were quantified using flow cytometry according to their cell-surface markers. Antibodies for CD45, CD3, CD4, CD8 and live/dead dye were used to analyses target cells.

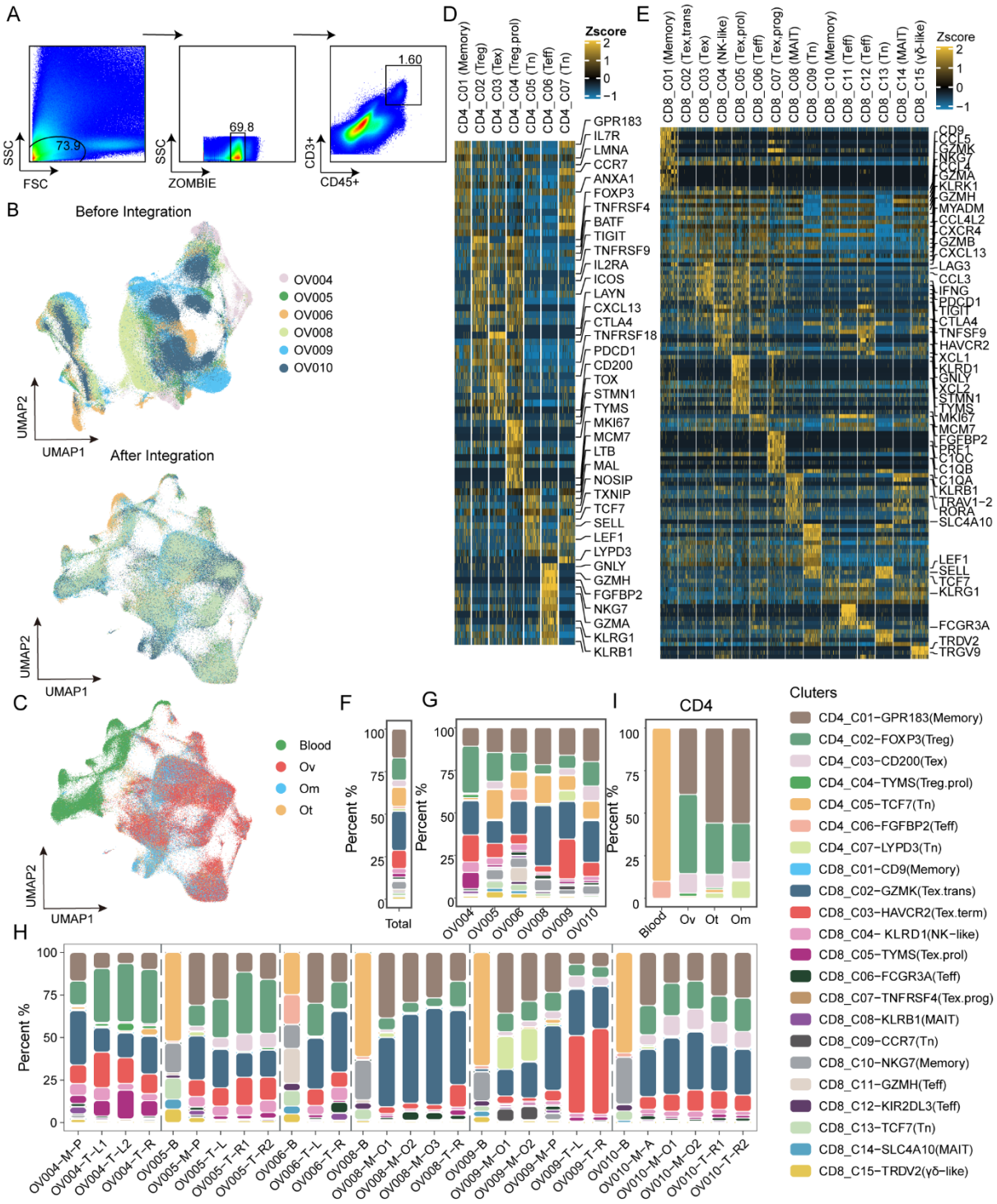

Figure S2. Distinct characteristics and differential composition of TILs across different lesions in HGSOC by scRNA-seq. Related to Figure 2.

A. T cells, were sorted using flow cytometry according to their cell-surface markers. Antibodies for CD45, CD3, and zombie dye were used to enriched target cells. **B**. Uniform manifold approximation and projection (UMAP) of 227,769 single CD3+ T cells colored by patient identity before and after CCA integration. **C.** UMAP of $CD3^{+}$

T cells showing the formation of positions where the cells from, including blood and solid tumor lesions, which including ovarian (Ov), omental (Om), and other distant metastatic (Ot). **D-E.** Heatmap of differentially expressed genes between cells belonging to each $CD4^+$ cluster and $CD8^+$ cluster. **F-H.** Bar plot indicating relative proportions of each cell cluster detected in total $CD3^+$ T cells, in different patients, and in different samples. **I.** Bar plot indicating relative proportions of each $CD4^+$ T cell cluster detected in blood and solid tumor lesions, including ovarian (Ov), omental (Om), and other distant metastatic (Ot). M_A = abdominal metastasis; M_P = pelvic metastasis; M_O = omental lesions; T_L= left ovarian lesions; T_R = right ovarian lesions.

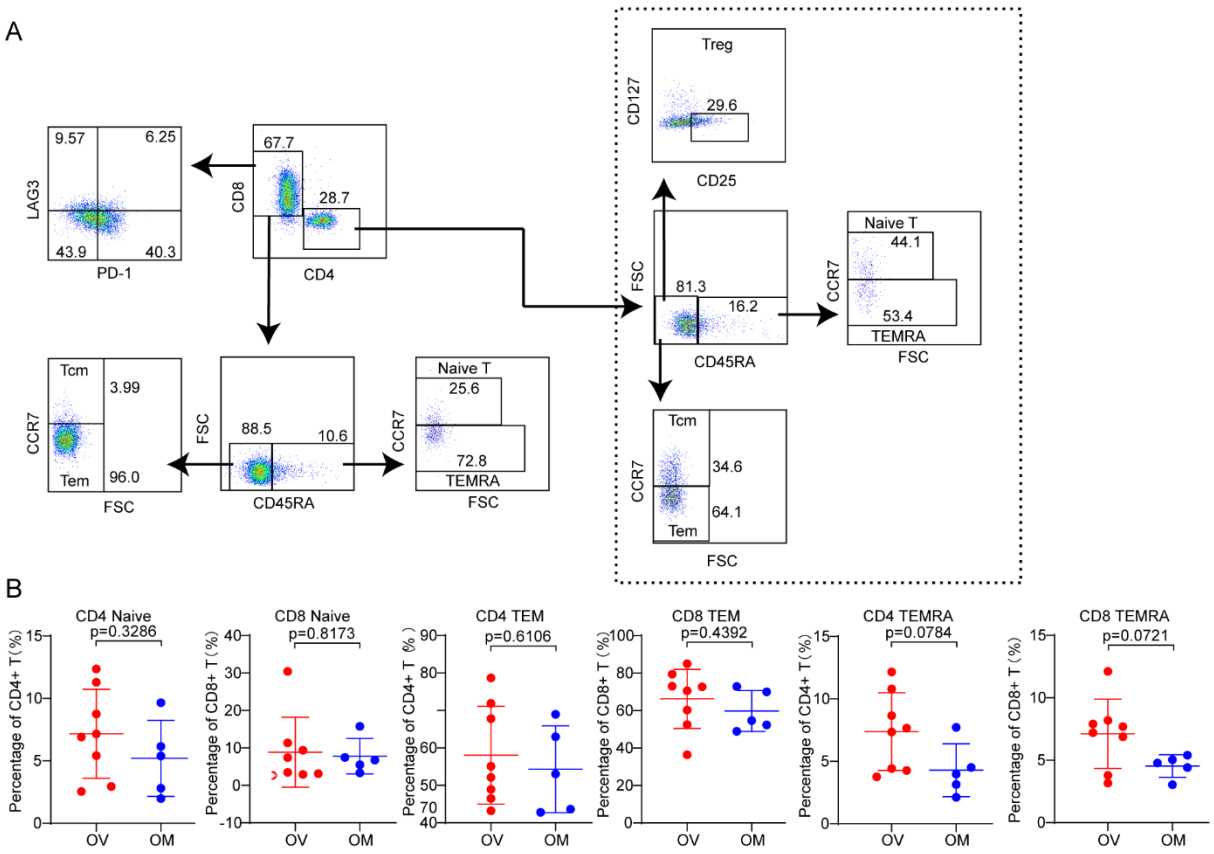

Figure S3. Flow cytometry analysis of the composition of T cell clusters in different lesions. Related to Figure 2.

A. Flow cytometry analysis of CD8+ and CD4+ T cell clusters. Representative graphs showing gating strategy.

B. Quantification of CD4+ naïve (CD45+CD3+CD4+CD45RA+CCR7+), TEM (CD45+CD3+CD4+CD45RA-CCR7-), TEMRA (CD45+CD3+CD4+CD45RA+CCR7-) and CD8+ naïve (CD45+CD3+CD8+CD45RA+CCR7+), TEM (CD45+CD3+CD8+CD45RA-CCR7-), TEMRA (CD45+CD3+CD8+CD45RA+CCR7-) cells proportions in tumors from each sample, respectively. ovarian samples=8, omental samples=5. p values were determined by student't test.

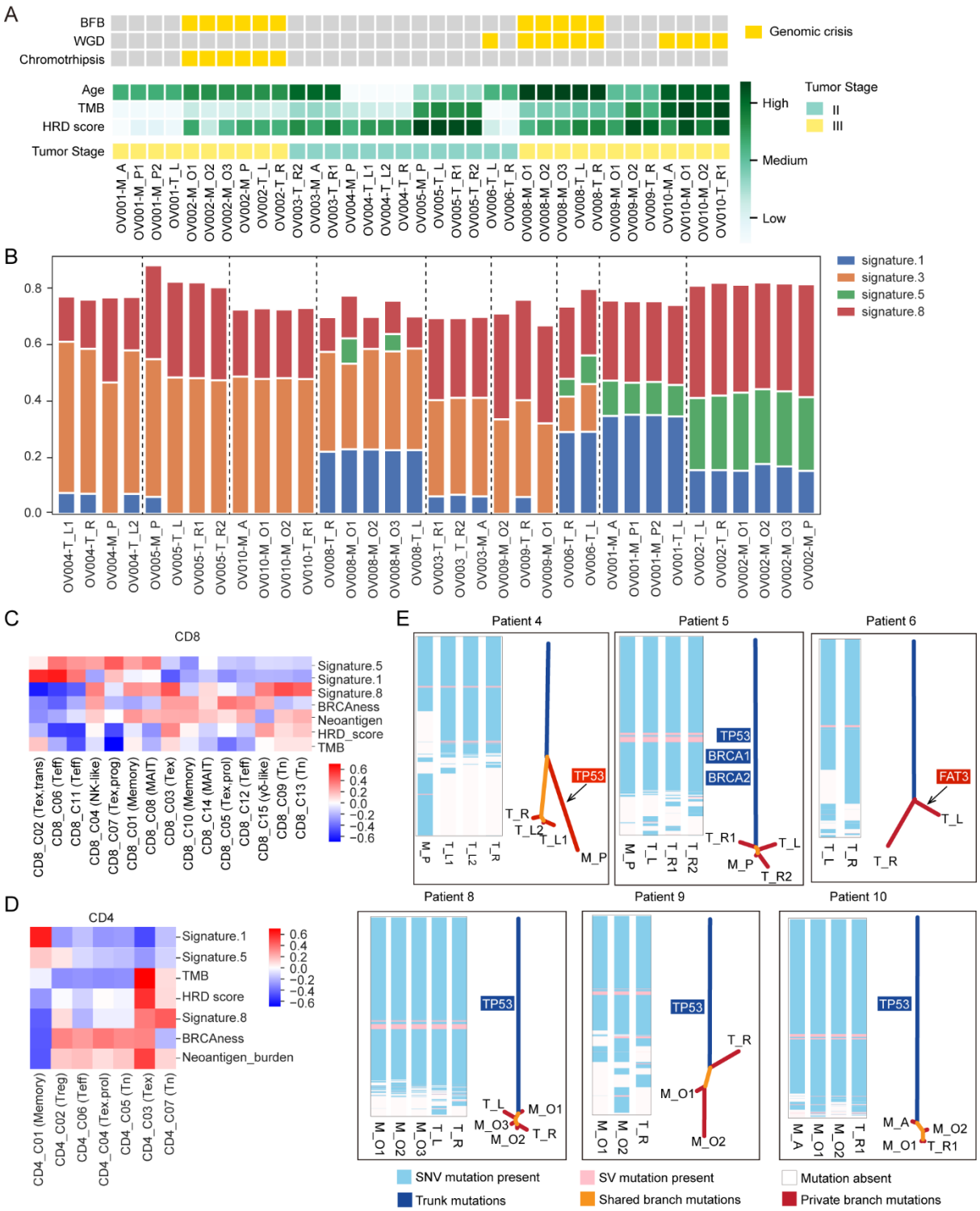

Figure S4. Patient derived TMB difference is associated with skewed T cell differentiation. Related to Figure 3.

A. The panels exhibit clinal information and genomic crisis events in each sample. BFB = breakage-fusion-bridge, WGD = whole genome duplication, TMB = tumor mutation burden, HRD = homologous recombination deficiency. **B**. The distribution of mutational signatures among tumor regions. **C-D**. Correlation between the cell

proportion of $CD8^+$ (**C**), $CD4^+$ (**D**) populations and the genomic features, including mutational signatures, TMB, HRD score. **E**. The evolutionary tree for each patient. M_A = abdominal metastasis; M_P = pelvic metastasis; M_O = omental lesions; T_L = left ovarian lesions; T_R = right ovarian lesions.

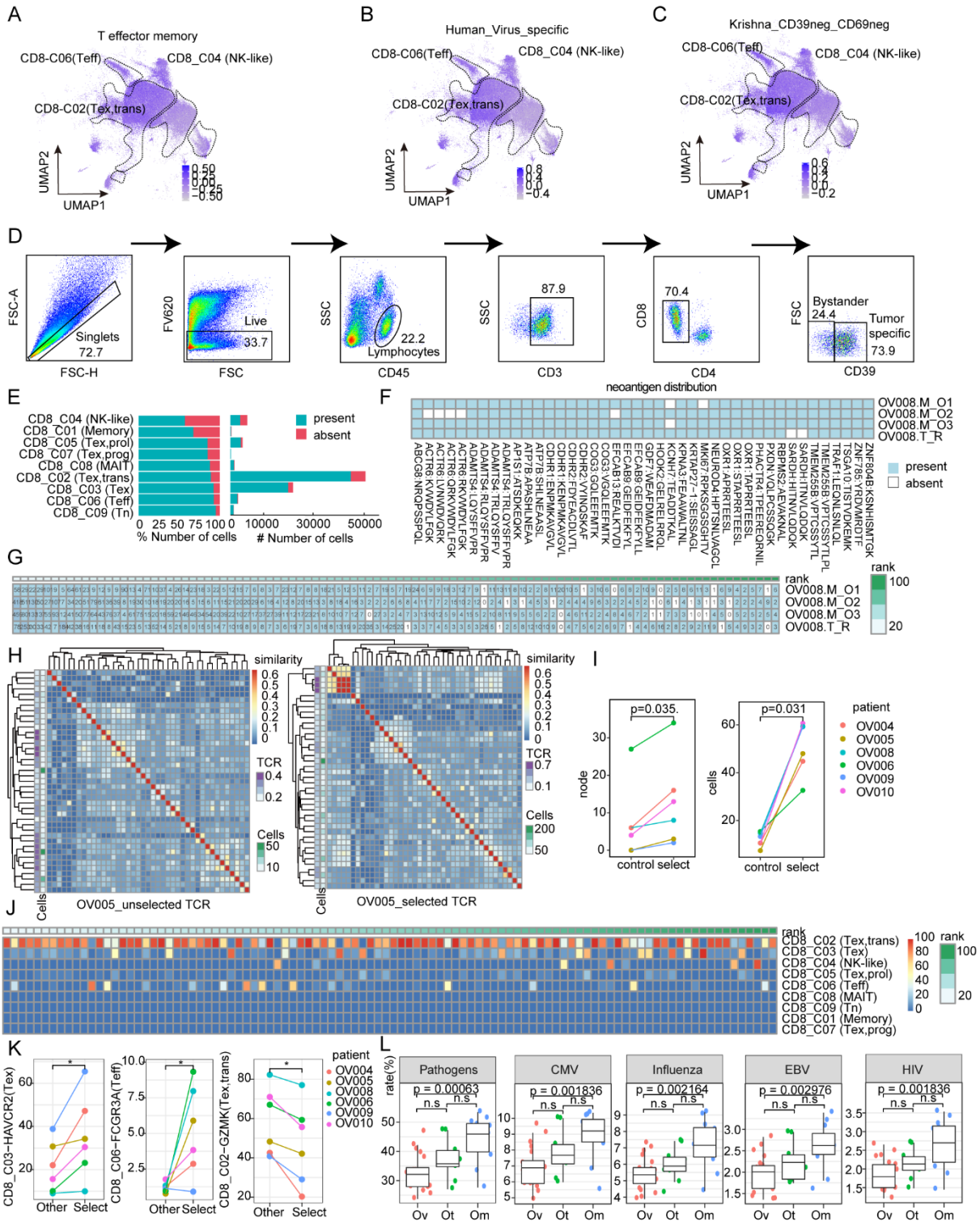

Figure S5. Characterization of CD8$^+$ tumor-infiltrating T cells in HGSOC. Related to Figure 3.

A-C. UMAP of CD8$^+$ tumor-infiltrating cells colored according to different gene signatures scores. (A) T effect memory signature score, (B) human virus specific signature score, (C) CD39$^-$CD69$^-$ signature score. **D.** Flow cytometry analysis of CD8$^+$ bystander and tumor-specific T cell clusters. Representative graphs showing gating strategy. **E.** Bar plots indicating relative proportions (left) and cell number (right) with or without TCR in tissue

$CD8^+$ clusters. **F**. MHC class I restricted neoantigens peptides were predicted from the data of WGS. Image of the neoantigens distribution in OV008 patient. **G.** The distribution of TOP100 clonal TCR across the sites. The number in each square stands for the same TCR cell number. **H.** The pairwise similarity of CD8 TCRs among selected neoantigen-associated (right panel) and control (left panel) from patient OV005. Unique CDR3 (α and β chain) sequences are arranged across rows and columns. The similarity was calculated by sharing of triplet amin acids in CDR3. The color showing similarity in the heatmap was restricted with less than 0.6 similarity. **I.** Comparison of similarity and cells between "select" and control. The mean of cell count of TCR in each patient. The pairwise TCR sequences with the similarity with more than 0.5 were connected and satisfied TCRs in select or control group created a network. In the network, the nodes were counted in each patient for select and control groups, respectively. Wilcoxon rank-sum test was performed. **J.** Representative image of distributions of cell clusters with top 100 clonal TCRs. **K**. The proportions of selected neoantigen associated TCRs and other TCRs in three T cell clusters. All T cells were divided into selected TCRs and remaining others. The selected TCRs were inferred in terms of the presence of neoantigens. Wilcoxon rank-sum test was performed. **L**. The content of disease-associated TCRs derived from bulk-TCR data in each sample. Top 9000 CDR3 of beta chain ranked by frequency were used to examine the disease-associated TCRs from three database: VDJdb, McPAS-TCR and TBAdb. Wilcoxon rank-sum test was performed.

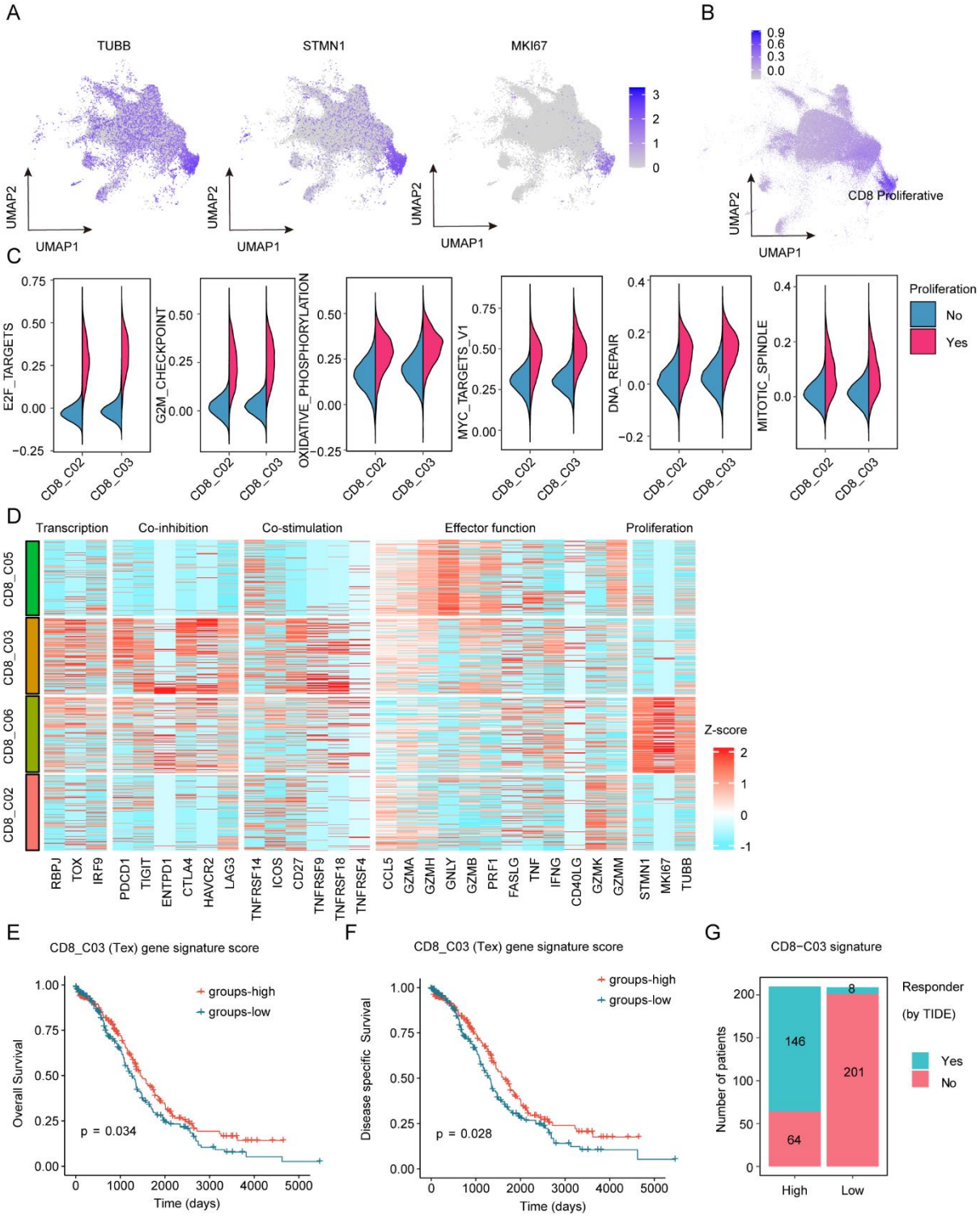

Figure S6. Characterization of proliferative CD8⁺ tumor-infiltrating cells. Related to Figure 4.

A. UMAP of all CD8⁺ tumor-infiltrating cells colored by proliferation markers. **B.** UMAP of all CD8+ tumor-infiltrating cells colored by proliferation signature. **C.** Comparation of gene signatures between T cells with and without proliferation in CD8_C02 and CD8_C03 clusters. each color represents a proliferation state. **D.** Heatmap depicting the expression of a panel of T cell related genes. **E-F** The Kaplan-Meier overall survival (**E**)

and disease specific survival (**F**) curves of TCGA ovarian cancer patients grouped by the gene signature expression (divided by the median value of the CD8_C03 gene signature score) of CD8_C03 (Tex) cluster. **G.** TCGA ovarian patients with good or poor ICB response were evaluated by TIDE (see methods) and then were grouped by the gene signature expression (divided by the median value of the CD8_C03 gene signature score) CD8_C03 (Tex) cluster.

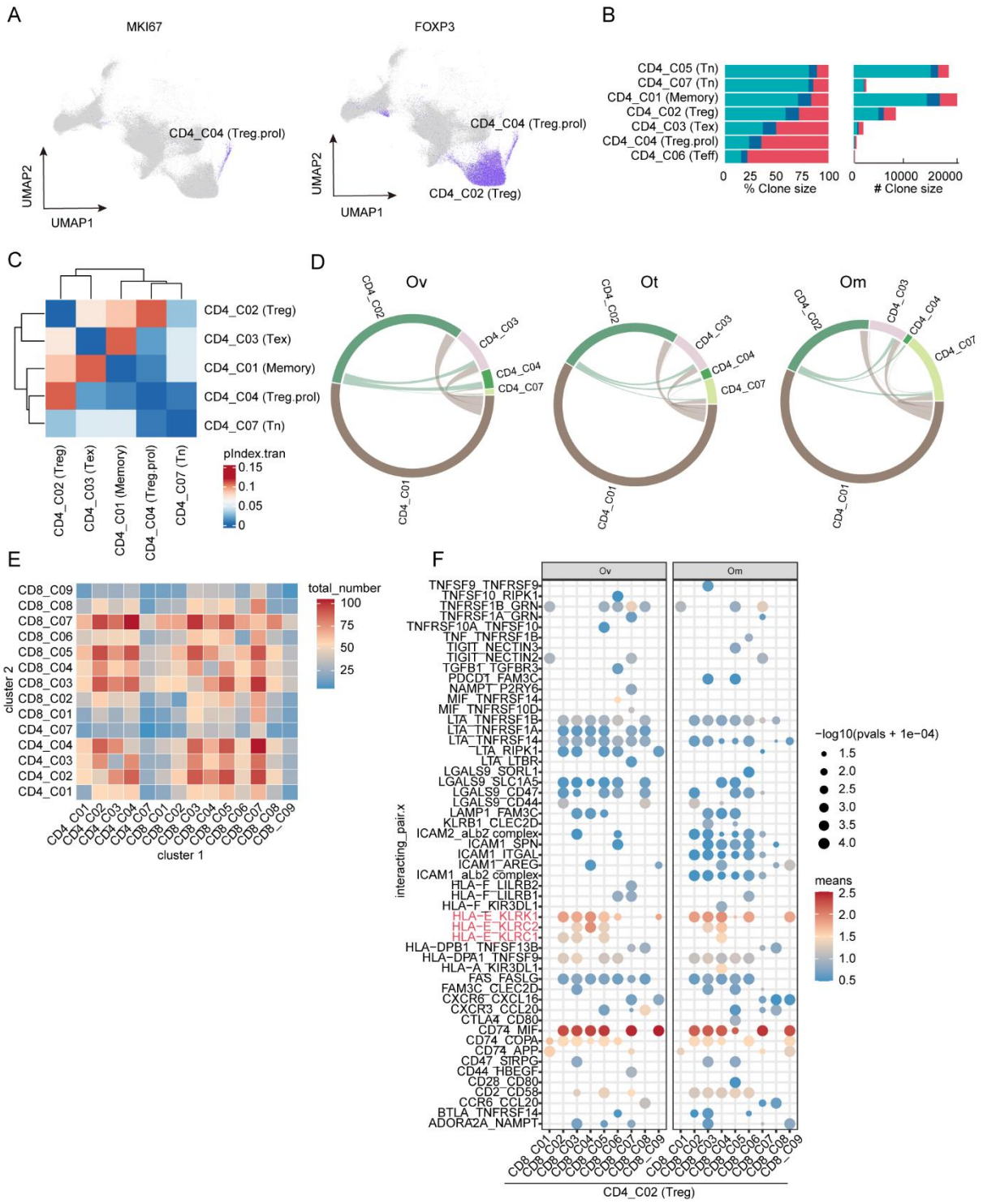

Figure S7. Characterization of TCR of CD4⁺ cells in HGSOC. Related to Figure 6.

A. UMAP of all CD8⁺ tumor-infiltrating cells colored by *MKI67* and *FOXP3*. **B.** Bar plots indicating relative proportions (left) and number (right) of TCR with different clone size. **C.** Heatmap showing the transition of all CD4⁺ tumor-infiltrating cells quantified by pSTARTRAC-trans indices for each patient (n = 6). **D.** Circle plot of clonal sharing between clusters in all CD4⁺ tumor-infiltrating cells in different solid tumor sites,

including ovarian (Ov), omental (Om), and other distant metastatic (Ot). The unique TCRs within each cluster were not shown. **E**. Heatmap of cluster-specific receptor-ligand interactions inferred by CellPhoneDB. Color indicates the total number of receptor and ligand genes pairs between each two TIL clusters. **F.** Heatmap of cluster-specific receptor-ligand interactions inferred by CellPhoneDB. Shown are inferred interactions between CD4_C02 (Treg) cluster and all TIL $CD8^+$ T clusters in ovarian (Ov) and omental (Om). Circle size indicates significance of interaction and circle color indicates mean expression of receptor and ligand genes for each pair.

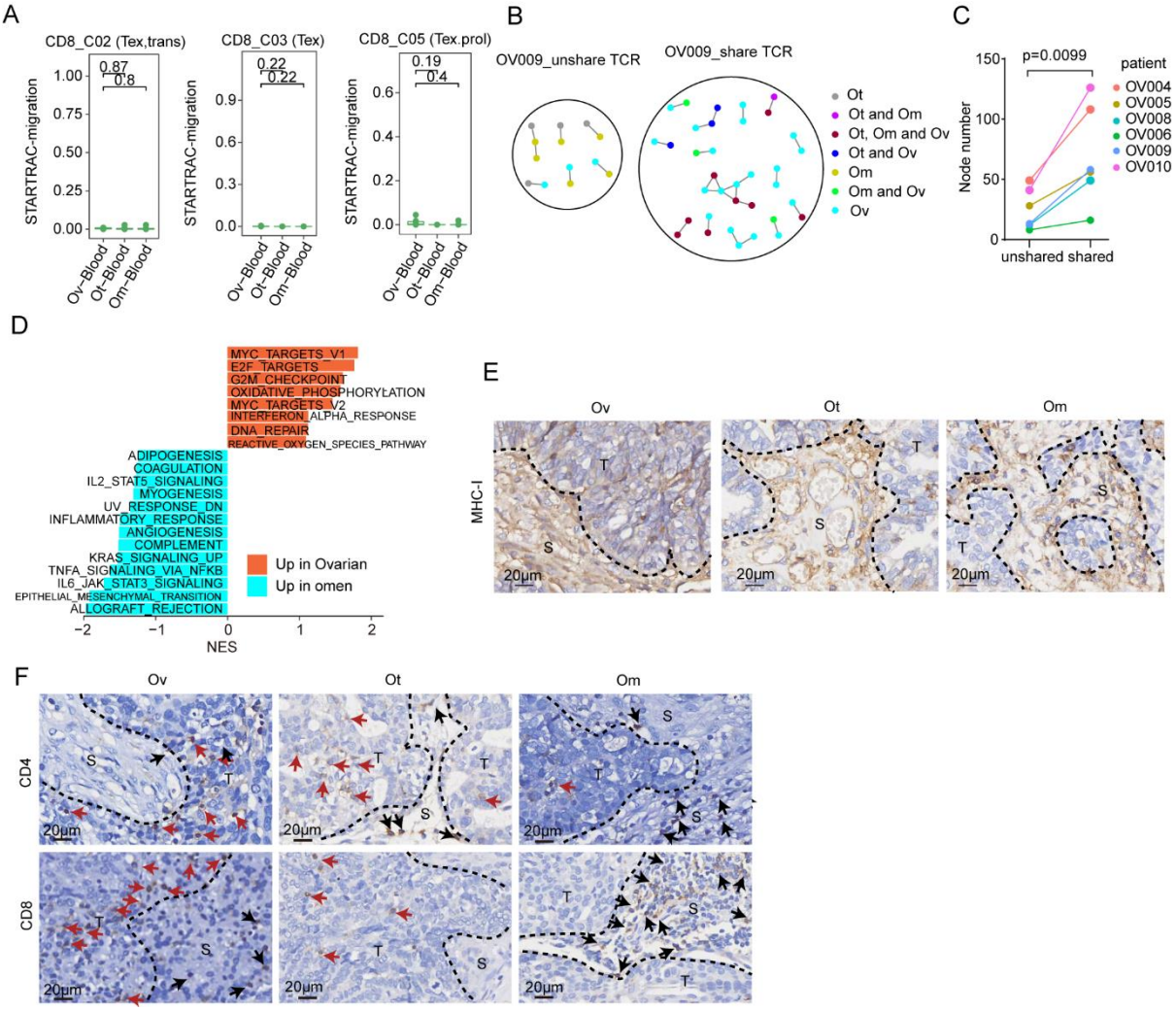

Figure S8. TCR from different sites of CD8⁺ tumor-infiltrating cells. Related to Figure 7.

A. Developmental migration of CD8⁺ tumor-infiltrating cells between blood and each solid tumor sites quantified by pSTARTRAC-migr indices for each patient (n = 6), Kruskal–Wallis test. **B**. Network diagrams showing shared between transitional cluster (CD8_C02) and dysfunctional clusters (CD8_C03 and CD8_C05) and unshared TCR sequences that have the similarity more than 0.5 to at least one of other TCRs for OV009. The similarity was calculated by sharing of triplet amin acids in CDR3 (both α and β chains). **C**. The number of nodes of the network diagrams were counted and compared in individual level. Paired t test. **D.** Analysis of significantly differentially regulated pathways between ovarian and omental sites on bulk RNA-seq data by GSEA. **E**. Representative images of IHC with MHC-I in tumor tissues (200x). Dotted line indicated the margin

of the tissues. T=tumor, S=stromal. **F.** Representative images of IHC with CD4 and CD8 in tumor tissues (200x). Red arrows indicate typical T cells in tumor area and black arrows indicate typical T cells in stroma area. Dotted line indicated the margin of the tissues. T=tumor, S=stromal.

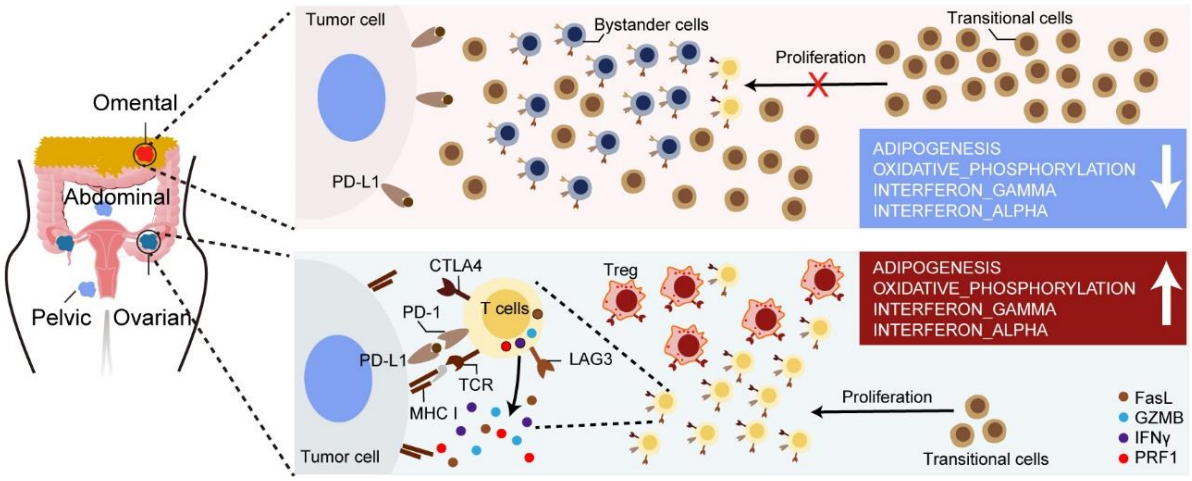

Figure S9. | Proposed model of detailed immune landscape across different lesions in HGSOC. Related to Figure 7.

Ovarian tumors were characterized by an immunosuppressive environment consisting of Tregs and three different populations of exhausted $CD8^+$ T cells as well as an exhausted $CD4^+$ T cell population that likely acquired an exhausted phenotype through interaction with tumor antigens in the local ovarian ecosystem (bottom). Omental lesions appear to consist primarily of non-tumor-specific bystander cells with no response to tumor specific antigens (upper). Increased expression of MHC-I, adipogenesis and interferon signaling and E2F mediated differentiation may contribute to high level of exhausted T cells in ovarian tumor sites.